Improved Slotted Disk Type Velocity Selector for Molecular Beams*

HANS U. HOSTETTLER AND RICHARD B. BERNSTEIN
Chemistry Department, University of Michigan, Ann Arbor, Michigan
(Received May 12, 1960; and in final form, June 2, 1960)

A slotted disk type mechanical velocity selector, 10 cm long and 16 cm in diameter, consisting of six disks has been constructed and tested. The velocity resolution corresponding to the half-intensity width is 0.047; no velocity sidebands are transmitted. The effective fractional open time to the incident beam is 0.35. At the highest rotor speed used (17 000 rpm) the transmitted velocity is 1.05×10^5 cm/sec. A general theoretical analysis of the transmission and resolution of selectors with disks of finite thickness is presented. The velocity distribution is reported for a molecular beam effusing from an oven equipped with Zacharias corrugated foil exit canals.

INTRODUCTION

VELOCITY selectors consisting of rotating cylinders provided with many helical grooves have been widely used to obtain monoenergetic molecular beams or neutron beams.[1–3] Although the milling of the helical slots involves considerable effort, the resulting selector is characterized by a high transmission and the complete absence of velocity "sidebands." These sidebands are a common problem with the mechanically simpler type of selector which consists of two or more slotted disks. In order to restrict the sidebands to contain only components from far out on the velocity distribution curve, the spacing between slots has been increased,[4] but this technique results in a considerable reduction in the transmitted intensity.

In the present paper a velocity selector consisting of six slotted disks is described. By using relatively thick disks, properly spaced, the velocity-selected beam is completely free of sidebands. The transmission of the rotor is still comparable to that for a grooved cylinder selector of similar resolution. The advantages of the present design are: (1) The rotor is relatively light (with a low moment of inertia) and can therefore be accelerated to high angular speeds. This speed advantage allows for smaller rotor length and thus more intense transmitted beams. (2) The disks have straight perpendicular slots and are easy to fabricate. (3) The selector is suitable for use with beams of permanent gases as well as condensable vapors; most of the molecules of the "wrong" speed are effectively removed from the beam direction by collision with the face of a disk rather than with the sidewall of a groove.

DESIGN OF THE VELOCITY SELECTOR

The design of the rotor and the method of elimination of the "sidebands" are illustrated in Fig. 1. This drawing shows the "unrolled" surface of the rotor. In this representation trajectories of molecules are straight lines. The tangent of the angle of inclination of the line is proportional to the molecular speed. Molecules of the desired velocity are transmitted by passing through those slits of the end disks which are displaced (rotated) through the angle ϕ. The intermediate disks must be placed so as to interrupt all trajectories of the wrong pitch (which would lead to sidebands).

The geometry of the rotor may be characterized by the parameters

$$\beta=d/L, \tag{1}$$

$$\gamma=l_1/r\phi, \tag{2}$$

and

$$\eta=l_1/(l_1+l_2). \tag{3}$$

Here β is the ratio of the disk thickness d to the length L of the rotor and γ is the ratio of the slit width l_1 to the length of the arc subtended by ϕ. The quantity η is the fractional open area expressed in terms of l_1 and l_2, the wall thickness between slits. Since the slits are of finite length, extending over a small range of the radius r, the wall thickness varies slightly from one end of the slit to the other; here, l_2 represents the average value.

It is important to place the disks so as to permit easy alignment in the assembly of the rotor. In projecting the disks along the rotor axis, it is desirable that the slits either coincide or fall exactly between one another. Thus ϕ should satisfy the equation

$$\phi r=n\bar{l}, \tag{4}$$

where $\bar{l}=(l_1+l_2)/2$ and n is an integer. For convenience the horizontal axis of Fig. 1 is marked in units of $\bar{l}$.

Since γ is dependent on ϕ (Eq. 2), the choice of γ is restricted to discrete values according to the formula

$$\gamma=2\eta/n. \tag{5}$$

The design of the present rotor is based on the values $n=15$, $\eta=\frac{1}{2}$, and $\beta=0.0163$, so that $\gamma=1/15=0.0667$. For the actual disks used, the relation $l_1=l_2$ is true only at the base of the slits. However, in connection with the problem

* Financial support from the Alfred P. Sloan Foundation and the U. S. Atomic Energy Commission, Division of Research, is gratefully acknowledged.

[1] R. C. Miller and P. Kusch, Phys. Rev. **99**, 1314 (1955).
[2] J. G. Dash and H. S. Sommers, Jr., Rev. Sci. Instr. **24**, 91 (1953).
[3] E. F. Greene, R. W. Roberts, and J. Ross, J. Chem. Phys. **32**, 940 (1960).
[4] P. M. Marcus and J. H. McFee in *Recent Research in Molecular Beams*, edited by I. Estermann (Academic Press, Inc., New York, 1959).

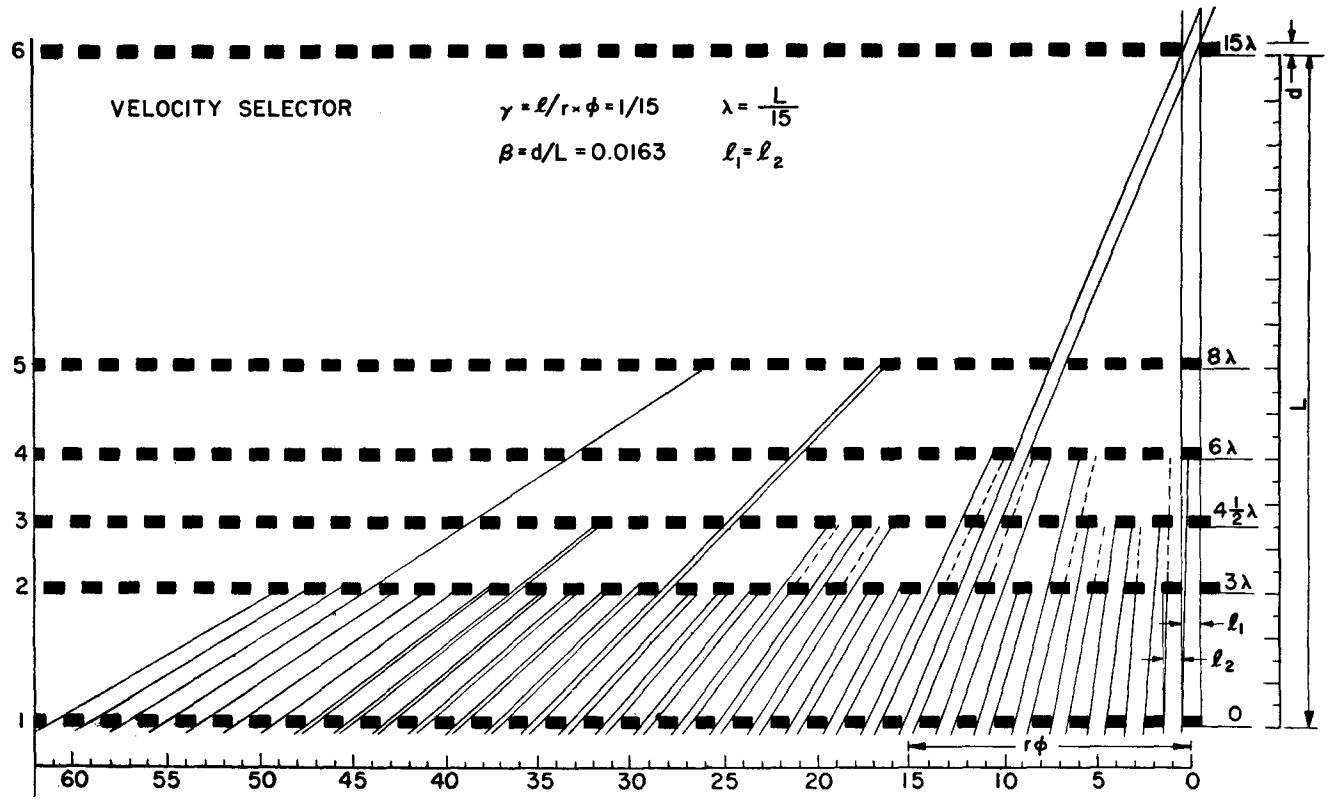

FIG. 1. "Unrolled" rotor showing location of disks for sideband elimination.

of elimination of sidebands this is the least favorable case and has therefore been chosen for Fig. 1. For subsequent calculations of the transmission and resolution of the velocity selector, the slightly smaller average values for γ and η will be used.

The condition of easy alignment also limits the possible locations of the intermediate disks to $n-1$ positions (here 14), which are indicated on the vertical axis of Fig. 1 in units of $\lambda = L/n$. By a process of trial and error it appeared that the minimum number of intermediate disks needed to eliminate all sidebands is four, and that one disk must be placed at a position corresponding to a half-integer λ. The most convenient combination is the one shown in the figure, with intermediate disks at positions 3, $4\frac{1}{2}$, 6, and 8λ.

It is seen from the figure that finite disk thickness is essential for effective blocking of all sidebands. It is noted first that disk 1 itself eliminates all sidebands of higher order than $1/\beta$ (here 62.5); a special case in point is the trajectory originating from position 35 which is effectively blocked by the sidewalls of the slits of disk 5.

TRANSMISSION AND RESOLUTION

Figure 2 is a similar representation to Fig. 1, showing only the two end disks. The transmitted beam packages consist of molecules within a defined velocity bandwidth. The limiting velocities correspond to the trajectories marked v_{max} and v_{min} in Fig. 2(a); v_0 is the nominal velocity for a given setting of the angular speed ω of the rotor. Equating the transit time of a molecule of speed v_0 with the time required for the rotor to turn through the angle ϕ, one obtains

$$v_0/L = \omega/\phi. \tag{6}$$

Similarly, a molecule with velocity v_{max} travels the distance $L-d$ during the time the rotor turns by the angle $\phi - l_1/r$, so that

$$v_{max}/(L-d) = \omega/(\phi - l_1/r).$$

By the same reasoning,

$$v_{min}/(L+d) = \omega/(\phi + l_1/r).$$

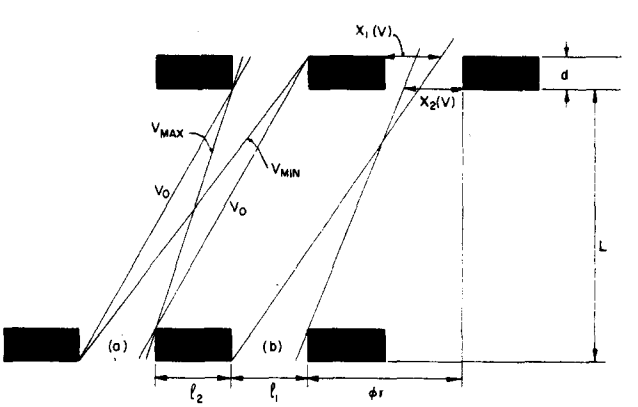

FIG. 2. (a) Representation of v_{max} and v_{min}; (b) diagram used in deriving transmission function.

Thus, substituting ϕ from Eq. (6), letting $\beta=d/L$, one obtains

$$v_{\max}=v_0\left(\frac{1-\beta}{1-\gamma}\right), \tag{7a}$$

where

$$v_{\min}=v_0\left(\frac{1+\beta}{1+\gamma}\right). \tag{7b}$$

The transmission of the rotor is

$$T=\int_{v_{\min}}^{v_{\max}} I(v)B(v)dv \tag{8a}$$

$$\cong I(v_0)\int_{v_{\min}}^{v_{\max}} B(v)dv, \tag{8b}$$

where $B(v)$ is the effective slitwidth (admittance) for different velocities and $I(v)$ is the velocity distribution of the incident beam. Other authors have indicated[1] that the error is small if one assumes a homogeneous distribution within the small velocity range admitted for a given ω. Thus in Eq. (8b) $I(v)$ is replaced by $I(v_0)$.

It is seen from Fig. 2(b) that $B(v)$ is given by

$$B(v)=\eta[1-x_{1,2}(v)/l_1], \tag{9}$$

where x_1 or x_2 is applicable if v is less than or greater than v_0, respectively. Equations for x_1 and x_2 are obtained [with the aid of Fig. 2(b)] as follows:

$$v/(L+d)=\omega/(\phi+x_1/r);\quad v/(L-d)=\omega/(\phi-x_2/r).$$

Eliminating x_1 and x_2 from Eq. (9), one obtains

$$B(v)=\eta\{1-[(1+\beta)v_0/v-1]/\gamma\} \text{ for } v_0>v>v_{\min} \tag{10a}$$

and

$$B(v)=\eta\{1+[(1-\beta)v_0/v-1]/\gamma\} \text{ for } v_{\max}>v>v_0. \tag{10b}$$

For v outside the range $v_{\min}$ to $v_{\max}$, $B(v)$ is zero.

The integration in Eq. (8b) is carried out in two parts, from $v_{\min}$ to v_0 and from v_0 to $v_{\max}$, resulting in the equation

$$T=I(v_0)\eta v_0\gamma^{-1}\{(1+\beta)\ln[(1+\beta)/(1+\gamma)] + (1-\beta)\ln[(1-\beta)/(1-\gamma)]\}. \tag{11}$$

For β and γ small compared to unity, Eq. (11) is simplified to yield

$$T=I(v_0)\eta v_0\gamma(1-\beta/\gamma)^2=Gv_0I(v_0), \tag{12}$$

where $G=\eta\gamma(1-\beta/\gamma)^2$ is a geometrical factor. For infinitely thin disks $\beta=0$ and Eq. (12) becomes identical with Eq. (4) of footnote reference 1.

The function $B(v)$ has a nearly triangular shape with the peak at v_0, dropping to zero at $v_{\min}$ and $v_{\max}$. The resolution R corresponding to the half-intensity width amounts to

$$R=(v_{\max}-v_{\min})/2v_0=(\gamma-\beta)/(1-\gamma^2)\cong\gamma-\beta. \tag{13}$$

It can be shown that the *effective* fractional open time η' to the incident beam is given by $\eta'=\eta(1-\beta/\gamma)$. For the present selector $\eta'=0.35$.

These results are valid only for an infinitely narrow beam. The influence of a wide and disperse beam on the resolution has been investigated by other authors[2]; their treatment is also applicable to the present type of selector.

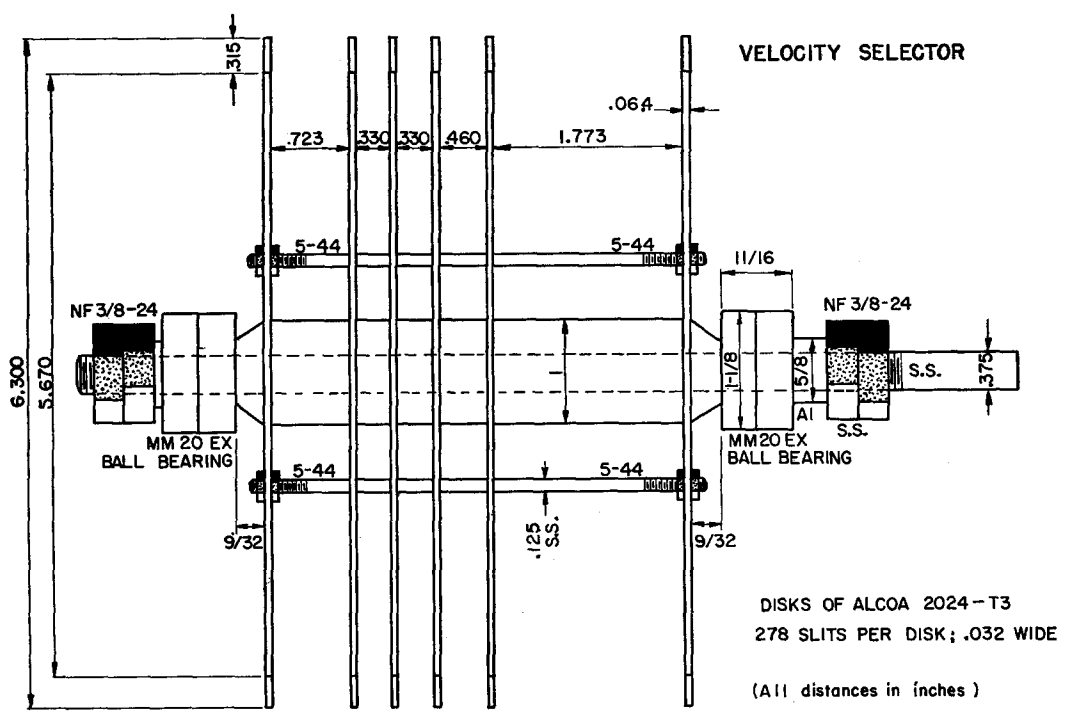

FIG. 3. Rotor assembly diagram.

TABLE I. Specifications of velocity selector.

Number of disks	6
Diameter of disks	16.0 cm
Number of slits per disk	278
Length of slits (in radial direction)	0.8 cm
Slit width, l_1	0.0813 cm
Wall thickness between slits	
At base of slits	0.0814 cm
At top of slits	0.0995 cm
Average value, l_2	0.0905 cm
Average radius, r	7.6 cm
Disk thickness, d	0.1628 cm
Over-all length of rotor, $L+d$	10.16 cm
L	9.997 cm
ϕ	0.1695 rad
γ (average)	0.0631
β	0.01628
η (average)	0.4732
G	0.0164
Resolution, R	0.0468

By the same method used earlier in this section, a formula has been derived to show the change in transmission caused by an inclination of the molecular beam to the rotor shaft by a small angle α, where α lies in the plane tangential to the disk periphery. Here the transmission T' turns out to be

$$T'=T(1-\delta)^{-2}\cong T(1+2\delta), \tag{14}$$

where $\delta=\alpha L/r\phi$. In a divergent beam (but one whose main direction is parallel to the rotor shaft), the effect is canceled to a large extent by negative and positive α, so that the influence on the total transmission is negligible.

DESCRIPTION OF THE INSTRUMENT

The present velocity selector is part of a molecular beam scattering apparatus, whose description will be published later.

Figure 3 is a schematic diagram of the rotor assembly. Figure 4 is a photograph of the entire velocity selector removed from the vacuum chamber. The principal specifications are listed in Table I.

The disks are made of Alcoa 2024-T3 aluminum alloy. Fifteen disks were clamped together between two heavy end disks; the milling of the slits was done on a horizontal mill, using a 0.032-in. thick circular carbide saw.

To facilitate alignment of the disks, prior to mounting them on the rotor shaft, a stack of six disks was formed and held together by a screw through their center holes. Then the disks were aligned in their relative positions according to Fig. 1 and checked with a magnifying glass. They were positioned so that the beam packages pass through slits which had been milled by the same cut, in order that small deviations or inaccuracies in the milling do not impair the performance of the selector. After the disks were thus aligned, they were clamped firmly and two $\frac{1}{8}$-in. holes drilled through the stack (at exactly opposite locations along a diameter). The disks were then mounted on the $\frac{3}{8}$-in. diam stainless steel rotor shaft with 1-in. diam aluminum spacer rings between them; $\frac{1}{8}$-in. stainless steel rods were passed through the alignment holes and fastened to the end disks by means of nuts. This disk assembly, together with the high speed precision ball bearings (Fafnir MM20EX CR) on both ends, was finally locked on the shaft by a pair of nuts on each end of the shaft (see Fig. 3).

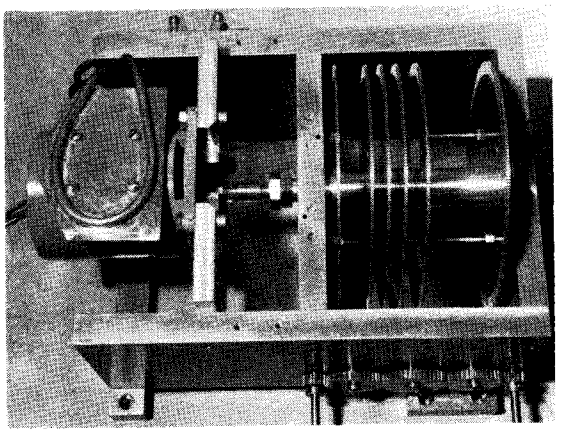

FIG. 4. Photograph of velocity selector (top view).

The rotor is directly coupled to a hysteresis synchronous motor (Syntorque type A 28H46) contained in the vacuum chamber. The motor is driven from a variable frequency power supply, consisting of a calibrated oscillator and a 120-w power amplifier.[5] The calibration of the oscillator may be rechecked at 75, 150, 300, and 600 cps (corresponding to 2250,$\cdots$18 000 rpm of the motor) by means of a built-in 600-cps tuning fork; the error in setting the oscillator for a desired frequency is $<0.5\%$. The four-pole synchronous motor is operated single phase, with an appropriate shifting capacitor used to supply the quadrature winding. Power factor correction (necessary when the frequency is varied appreciably) is accomplished by means of series and parallel capacitors. A neon bulb which is supplied with the same frequency as the motor serves as a stroboscope to check synchronization.

The rotor assembly can be lowered by about 1 cm and thus be moved out of the beam path. This is accomplished from outside the vacuum chamber by O-ring rotary seals. The motor, being stationary, is connected to the rotor shaft by a flexible coupling, consisting of a piece of Tygon tubing.

For the present selector the relation between rotor speed Ω (rpm) and the nominal velocity v_0 (cm/sec) is $v_0=6.177\Omega$. The highest speed obtained is 17 000 rpm corresponding to $v_0=1050$ m/sec. The casing of the motor was provided with a water cooling coil (visible in Fig. 4), but this turned out to be unnecessary; a thermocouple attached to the motor indicated no appreciable temperature rise during opera-

[5] Circuit diagrams for the power oscillator and capacitor network, with additional miscellaneous information is available on request from H. F. Schulte, Electrical Engineering Department, University of Michigan, Ann Arbor, Michigan.

tion. The enclosed ball bearings in the motor were greased in the factory with Mil G 3278 grease; the ball bearings (open type) for the disk assembly are lubricated regularly with DC 702 silicone pump fluid.

Two of these velocity selectors have been constructed and have operated without difficulty inside a vacuum chamber at pressures below 3×10^{-7} mm Hg.

MEASUREMENT OF TRANSMISSION

As a check on the operation of the velocity selector, the velocity distributions for beams of SO_2 and NH_3 have been measured.

The molecular beam effused from an oven equipped with Zacharias[6] crinkly foil exit canals. The gas flow into the oven is measured with an external burette maintained at constant pressure. The path length from the oven to the detector is 33 cm. The detector consists of an electron bombardment ionizer, electron multiplier, and cathode follower. The beam is mechanically modulated (at 25 cps); thus a tuned amplifier and a phase-sensitive detector are used.

It was desired to compare the observed transmission of the velocity selector with the calculated value. If one had a source which produced a beam with a perfect Maxwellian velocity distribution, one could simply compare the experimental and calculated transmission at any velocity. However, the beams obtained from the ovens used in the present experiments show a distorted velocity distribution, so that another method for checking the transmission was needed.

An electron bombardment ion source produces an ion current proportional to the particle density of the incident beam. The output signal $S(v)$ from the detection system with the velocity selector set for velocity v is thus

$$S(v)=CT(v)/v=CGI(v), \qquad \text{(15a, 15b)}$$

where C is an unknown proportionality factor. The transmission $T(v)$ is given by Eq. (12) and has been substituted in Eq. (15a) to give Eq. (15b). The signal S_0 coming from the direct velocity-*unselected* beam (measured by removing the velocity selector from the beam path) is

$$S_0=C\int_0^\infty I(v)/v\,dv. \qquad (16)$$

The elimination of $CI(v)$ from Eqs. (15b) and (16) gives

$$G=\int_0^\infty \frac{S/S_0}{v}dv=\int_0^\infty \frac{S/S_0}{v^*}dv^*. \qquad (17)$$

Here, the reduced velocity, $v^*\equiv v/\alpha$, [where $\alpha=(2RT/M)^{\frac{1}{2}}$] is introduced to provide a "universal" representation. Equation (17) can be used to evaluate G from a plot of measured values of $(S/S_0)/v^*$ vs v^* by graphical integration. Figure 5 is a typical curve of this type; the data are those of exp. 2 in Table II. The equation for the theoretical curve in Fig. 5 is obtained by substituting $I(v)=2v^3\alpha^{-4}\exp(-v^2\alpha^{-2})$ into Eqs. (15b) and (16). After elimination of C one obtains

$$\frac{S/S_0}{v^*}=\frac{4G}{(\pi)^{\frac{1}{2}}}v^{*2}\exp(-v^{*2}). \qquad (18)$$

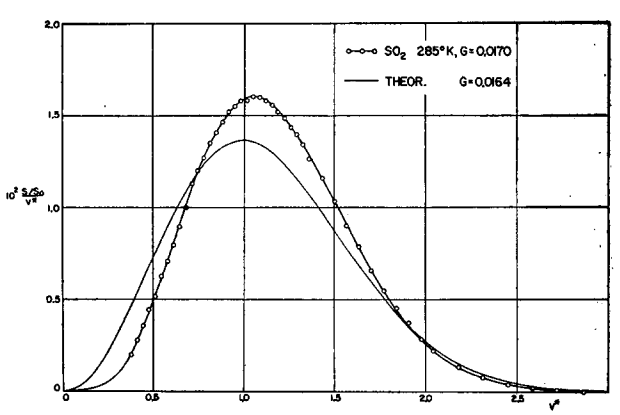

FIG. 5. Evaluation of geometrical factor G.

[6] J. R. Zacharias, Advances in Electronics and Electron Phys. 8, 19 (1956). The authors appreciate receiving a supply of crinkly foil from Professor Zacharias.

TABLE II. Experimental determination of G.

Exp	Gas	Oven temp (°K)	Flow rate to oven (cc (NTP)/hr)	10^2G
1	SO_2	285	22.7	1.66
2	SO_2	285	8.9	1.70
3	SO_2	285	3.25	1.72
4	SO_2	485	14.3	1.73
5	NH_3	285	28.0	1.70
				av 1.70±0.02

The results of the graphical integration of Eq. (17) for different experiments are presented in Table II. The average experimental value for G is 0.0170±0.0002 (a.d.). The deviation (3.7%) from the calculated value ($G=0.0164$) is to be noted. According to Eq. (14) a slight misalignment of the beam with respect to the rotor shaft direction by an angle $\alpha=8'$ could account for this difference.

APPLICATIONS

In molecular beam work velocity selectors are useful in connection with studies of elastic and inelastic scattering, for investigation of chemical reaction kinetics, and for studies of effusion of gaseous species from slits and orifices. As an example of the latter application, consider the results of the experiments mentioned in the previous section.

It is convenient to introduce a new reduced velocity, defined as

$$v'=v/(3/2)^{\frac{1}{2}}\alpha;$$

thus for effusion from an ideal slit or orifice the theoretical Maxwellian velocity distribution may be represented by

$$S/S_0 = (9v'^3/2)\exp(-3v'^2/2). \quad (19)$$

In Fig. 6 the experimental values of S/S_0 for one experiment (exp. 2 of Table II) are plotted versus v' for comparison with the theoretical curve [Eq. (19)]. The values of S/S_0 have been normalized so that the area under the curve is unity. Similar plots were obtained for other experiments at different flow rates (corresponding to different oven pressures).

It is seen from the figure that the beam is richer in intermediate velocities than predicted theoretically. The deficiency in low velocity molecules is at least partly due to cloud formation[7] in front of the oven exit canals; for reasons of beam intensity the operating pressures used in the oven were rather too high to expect pure Knudsen effusion. Experiments on the pressure dependence of the low velocity part of the distribution tended to confirm this view. However, the deficiency of the high speed molecules under the conditions of the present experiments is unexplained.

[7] R. D. Present, *Kinetic Theory of Gases* (McGraw-Hill Book Company, Inc., New York, 1958), p. 180ff.

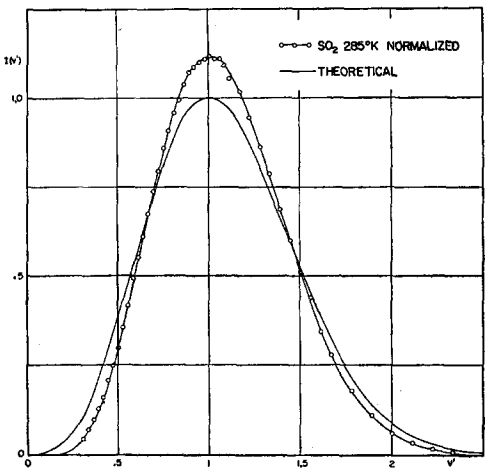

FIG. 6. Comparison of experimental and theoretical velocity distributions.

ACKNOWLEDGMENTS

Thanks are due our machinists, J. Mannlein and N Johnston, for their care in fabricating the slotted disks. The authors appreciate the cooperation of H. L. Schulte, who designed and constructed the electronic components. The authors also wish to thank F. A. Morse for his general assistance.